

On frequency dependence of pulsar linear polarization

P. F. Wang^{*}, C. Wang, and J. L. Han

National Astronomical Observatories, Chinese Academy of Sciences. A20 Datun Road, Chaoyang District, Beijing 100012, China

5 January 2015

ABSTRACT

Frequency dependence of pulsar linear polarization is investigated by simulations of emission and propagation processes. Linearly polarized waves are generated through curvature radiation by relativistic particles streaming along curved magnetic field lines, which have ordinary mode (O-mode) and extra-ordinary mode (X-mode) components. As emitted waves propagate outwards, two mode components are separated due to refraction of the O mode, and their polarization states are also modified. According to the radius to frequency mapping, low frequency emission is generated from higher magnetosphere, where significant rotation effect leads the X and O modes to be separated. Hence, the low frequency radiation has a large fraction of linear polarization. As the frequency increases, emission is generated from lower heights, where the rotation effect becomes weaker and the distribution regions of two modes are more overlapped. Hence, more significant depolarization appears for emission at higher frequencies. In addition, refraction effect of the O mode becomes serious in very deep magnetosphere, which bends the O mode emission towards outer parts of a pulsar beam and also causes the separation of mode distribution regions and hence the fractional linear polarization increasing with frequency. If emission of different frequencies is generated from a region of the same height, serious O mode refraction can result in the decrease of both profile width and fractional linear polarization. The observed frequency dependence of linear polarization for some pulsars can be naturally explained within the scope of our scenario.

Key words: magnetic fields - plasmas - polarization - pulsars: general - stars:rotation

1 INTRODUCTION

Pulsars are generally believed to be rapidly rotating neutron stars. Their polarized emission has been observed over a wide frequency range from about 100 MHz to 32GHz over more than forty years (e.g. Manchester 1971; Wu et al. 1993; Xilouris et al. 1996; Gould & Lyne 1998; Weltevrede & Johnston 2008; Han et al. 2009; Tiburzi et al. 2013). Very rich polarization features have been uncovered for both linear and circular polarizations, e.g., ‘S’-shaped position angle curves, orthogonal polarization modes, single sign and sign reversals of circular polarization, and their evolutions with frequency, etc. Linear polarization of average pulse profiles is predominant for most pulsars at low frequencies. The polarization percentage generally decreases with the increase of observing frequency (Morris et al. 1970; Manchester 1971). Manchester et al. (1973) noticed that some pulsars exhibit a critical frequency, below which the fractional linear polarization is constant, but above which it decreases with increasing frequency. To investigate the

change of pulsar polarizations across a much wider frequency range, Xilouris et al. (1996) extended polarization observations to mm-wavelengths, and noticed significant depolarization at high frequencies. Recently, Johnston et al. (2008) pointed out that simple profiles are more likely to be characterized by high linear polarization than complex profiles, and polarization properties for different profile components of a given pulsar behave differently with frequency, e.g., PSR J0922+0638.

In addition to analysis of polarization features for individual pulsars, statistical investigations were also undertaken for pulsar linear polarization. It has been noticed at early days that short period pulsars tend to have high linear polarization (Huguenin et al. 1971; Morris et al. 1981). Long period pulsars exhibit faster depolarization over frequency than the short period ones (Morris et al. 1981). Xilouris et al. (1995) presented the anti-correlation between the depolarization index and the acceleration potential near neutron star surface. Several authors also demonstrated that the degree of linear polarization is higher for a pulsar with a large spin-down luminosity \dot{E} (Qiao et al.

^{*} E-mail: pfwang@nao.cas.cn

1995; von Hoensbroech et al. 1998; Crawford et al. 2001; Weltevrede & Johnston 2008).

To understand various polarization features, numerous theoretical researches on pulsar polarization have been developed on the emission processes (e.g. Xu et al. 2000; Dyks et al. 2010; Wang et al. 2012; Kumar & Gangadhara 2012) or the propagation effects (e.g. Wang et al. 2010; Beskin & Philippov 2012), both of which can lead to depolarization. The depolarization of pulsar linear polarization is generally attributed to simultaneous interaction of two modes of orthogonally polarized radiation (McKinnon & Stinebring 1998; Karastergiou et al. 2005) or owing to randomization of position angles in weaker magnetic fields in outer magnetosphere (Manchester et al. 1975; Morris et al. 1981). For example, McKinnon (1997) attributed the depolarization to birefringence of the X mode and O mode above pulsar polar caps. von Hoensbroech et al. (1998) qualitatively explained depolarization at high frequencies by considering the evolution of one natural plasma mode within pulsar magnetosphere. However, the formation and distribution of the two modes within a pulsar beam were not mentioned; the refraction effect was simply discussed by analogy with the calcite crystal; the polarization limiting effect was simply analysed; and the evolution of linear polarization across field line planes was not investigated. To get a better understanding of the frequency dependence of pulsar linear polarization, emission processes together with propagation effects need to be investigated systematically.

Recently, we jointly studied the polarized curvature radiation together with propagation processes within pulsar magnetosphere numerically (Wang et al. 2014). We succeeded in demonstrating the distributions of the X-mode and O-mode within a pulsar magnetosphere and explained the depolarization across an entire pulsar beam. We found that the depolarization is serious if the corotation of relativistic particles is not considered. When the rotation is taken into account, significant linear polarization will be produced. However, the frequency dependence behaviour of linear polarization was not incorporated in the analysis.

Stimulated by the observational and theoretical investigations, we hereby develop the joint research of emission and propagation processes to understand frequency dependence of pulsar linear polarization by considering the polarized curvature radiation process together with propagation effects in a pulsar magnetosphere. In Section 2, we present theoretical basics for our calculations. Linearly polarized radiation within an entire pulsar beam, polarized pulse profile and their evolution with frequency are described in Section 3. Comparisons with observations are elaborated in Section 4. Discussions and conclusions are presented in Section 5.

2 THEORETICAL BASICS

2.1 Geometry and emission

Pulsar radio emission is generally believed to be generated by relativistic particles streaming out along the curved magnetic field lines within the open magnetosphere. Due to the bending of field lines, relativistic particles will experience perpendicular acceleration and produce curvature radiation. Coherent curvature radiation from bunches of relativistic

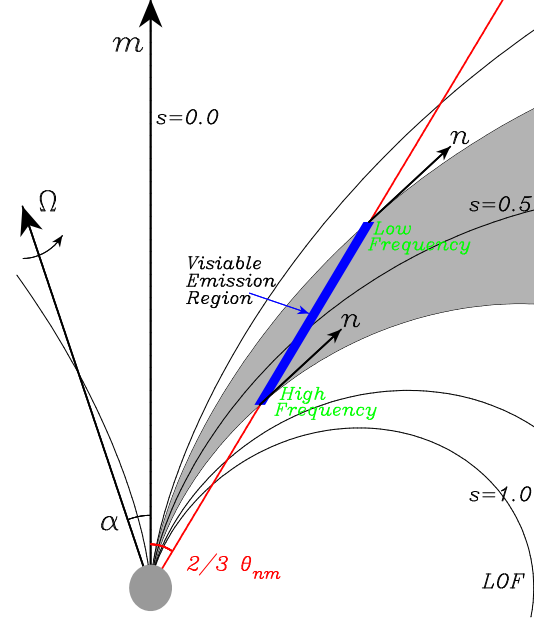


Figure 1. Emission regions on a bundle of magnetic field lines with $\theta \simeq 2/3\theta_{nm}$ for a given sight line. The magnetic moment \mathbf{m} is inclined by an angle of α with respect to the rotation axis Ω . The thick line outlines all tangential emission points of field lines. θ_{nm} represents the angle between the wave vector \mathbf{n} and the magnetic momentum \mathbf{m} . The grey area represents the region for outflowing relativistic particles along a bundle of magnetic field lines. $s = 0.0$ denotes the magnetic axis, $s = 1.0$ denotes the last open field line (LOF).

particles serves as one of the most probable mechanisms for pulsar radio emission. The coherent particle bunch can be treated as a point-like huge charge for the sake of simplicity. Pulsar magnetic fields are assumed to be of the static dipole form in the radio emission region,

$$\mathbf{B} = B_* \left(\frac{R_*}{r} \right)^3 [3\hat{\mathbf{r}}(\hat{\mathbf{r}} \cdot \hat{\mathbf{m}}) - \hat{\mathbf{m}}], \quad (1)$$

here B_* is magnetic field strength at the magnetic equator of a neutron star, R_* is the neutron star radius, $\hat{\mathbf{r}}$ is the unit vector along \mathbf{r} , and $\hat{\mathbf{m}}$ represents the unit vector of the magnetic dipole moment. Within the static dipole magnetosphere, emission generated from the regions of the same polar angle θ within a given magnetic field line plane will point towards the same direction, as shown in Fig. 1.

Along a field line, emission radiated at different heights has different frequencies. The characteristic frequency for curvature radiation reads,

$$\nu_{CR} = \frac{3\gamma^3 c}{4\pi\rho}. \quad (2)$$

Here, γ is the Lorentz factor of a relativistic particle, ρ represents the curvature radius for instantaneous particle trajectory. The larger curvature radius ρ for particle trajectory in the high magnetosphere naturally leads to lower frequency emission. This is the physical basis for the radius to frequency mapping.

For an inclined dipole magnetosphere, the pulsar emission beam is generally compressed in the meridional plane defined by the rotation axis and magnetic axis (Biggs 1990). For simplicity, our calculations assume that pulsar beams

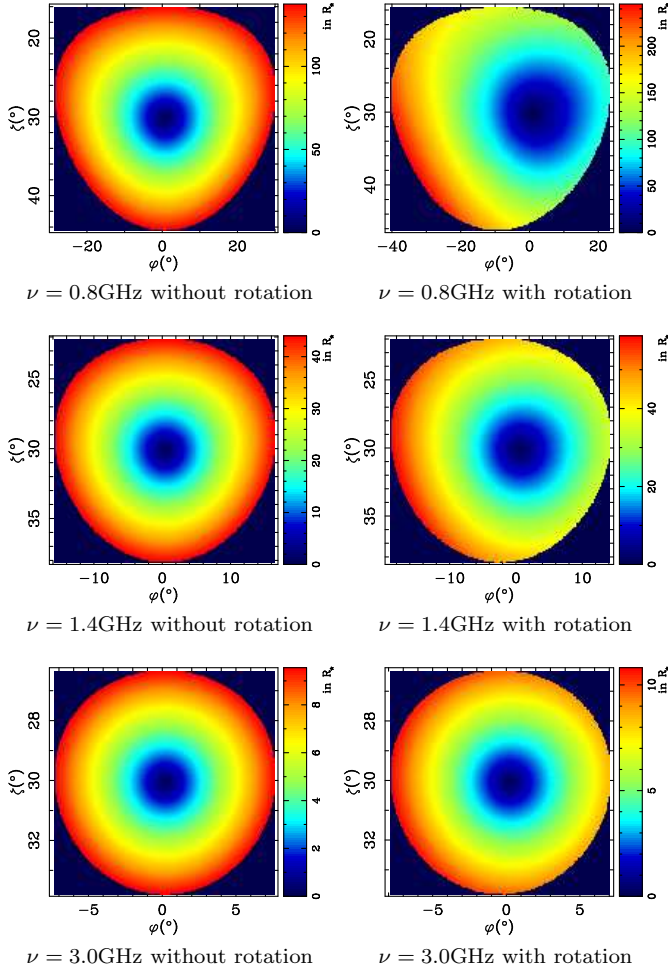


Figure 2. Emission heights (in the unit of R_*) for different frequencies in a pulsar beam, plotted in the rotation phase φ and the sight line angle ζ . Corotation of relativistic particles is not considered for the left panels, but considered for the right panels. The parameters used for model calculations are an inclination angle of $\alpha = 30^\circ$, a Lorentz factor of $\gamma = 500$, and a rotation period of a pulsar $P = 1$ s.

are circular, i.e., the last open field lines which define the boundary of a pulsar beam have the same field line constant of $r_{e, \text{lof}}$, as defined by equation (15) of Gangadhara (2004). In general, the beam size in the meridional direction does not affect our conclusions in this paper.

The emission regions at three different frequencies of ν_{CR} are calculated as shown in Fig. 2. The height ranges are quasi symmetric about the magnetic axis for emission at a given frequency generated from the static dipole magnetosphere. Emission near the beam centre comes from a lower altitude, as shown in the left panels of Fig. 2, because the curvature radii of the inner field lines at a lower altitude are comparable to those of the outer field lines at a higher altitude. Further, the entire emission regions get deeper in the magnetosphere for a higher frequency, which is caused by the smaller curvature radii of field lines in the deeper magnetosphere. It should be noted that relativistic particles within a pulsar magnetosphere not only stream along the curved magnetic field lines, but also corotate with magnetosphere. When the corotation is considered, the trajectories

and velocities of relativistic particles will be bent towards the rotation direction compared with those for the static dipole magnetosphere. Hence, the emission regions become asymmetry, with heights for the leading part of the beam getting larger than those for the trailing part, as shown in the right panels of Fig. 2.

For emission of a single particle bunch at a given height in the pulsar magnetosphere, the radiation field $\mathbf{E}(t)$ and the corresponding Fourier components $\mathbf{E}(\omega)$ can be calculated by using the circular path approximation, as described by Wang et al. (2012). The emission from a relativistic particle bunch is beamed in a $1/\gamma$ cone around the velocity direction. Therefore, the detectable emission from a given height and rotation phase is contributed by relativistic particles not only at the tangential emission point of a field line but also on nearby field lines within the $1/\gamma$ cone. By integrating the emission within an entire emission cone from all field lines, we will obtain the total polarized radiations in the given direction. In general, curvature radiation is highly linearly polarized, and the rotation has great influences on polarized curvature radiation process (Wang et al. 2014).

2.2 Propagation

Once polarized emission is generated through the curvature radiation process, they will be coupled to local plasma modes to propagate out in a pulsar magnetosphere, which is filled with relativistic plasmas that can be simply assumed to be cold (with a single Lorentz factor γ) and with a density of $N_p = \eta N_{\text{GJ}}$. Here, η is the multiplicity factor and N_{GJ} represents the Goldreich-Julian density (Goldreich & Julian 1969). Two eigen transverse modes, the X-mode and O-mode, of the plasma have been carefully investigated by Wang et al. (2010) and Beskin & Philippov (2012). The X-mode waves have a refraction index of $n_x = 1$ and propagate rectilinearly; while the O-mode waves have a refraction index of $n_o < 1$ and suffer refraction (Barnard & Arons 1986). The polarization states of the X-mode and O-mode change during their propagation. In the inner magnetosphere near the emission region, the polarization states of both modes evolve adiabatically, i.e., with the polarization of the X-mode wave orthogonal to the local $\mathbf{k} - \mathbf{B}$ plane and the polarization of the O-mode wave within the $\mathbf{k} - \mathbf{B}$ plane (Cheng & Ruderman 1979). As the waves propagate to the higher magnetosphere, the adiabatic condition is not satisfied and wave-mode coupling happens, i.e., one mode leaks to the other and vice versa. The altitude where the mode coupling happens is named as being the polarization limiting radius (Cheng & Ruderman 1979; Wang et al. 2010). Above the polarization limiting radius, the polarization states of both modes are frozen and will not be further affected by the plasma, except for possible cyclotron absorption in the outer magnetosphere.

In addition to evolution of a single wave mode, the distributions of polarized waves within each $1/\gamma$ emission cone also change during propagation. As shown by Wang et al. (2014), the O mode refraction will lead detectable X and O modes at a given position to be incoherent, as they originate from different parts of a pulsar beam. Adiabatic walking will result in the ordering of polarized waves within the $1/\gamma$ cone, i.e., with the O-mode wave vectors following the polarization plane of initial emission, but wave vectors for

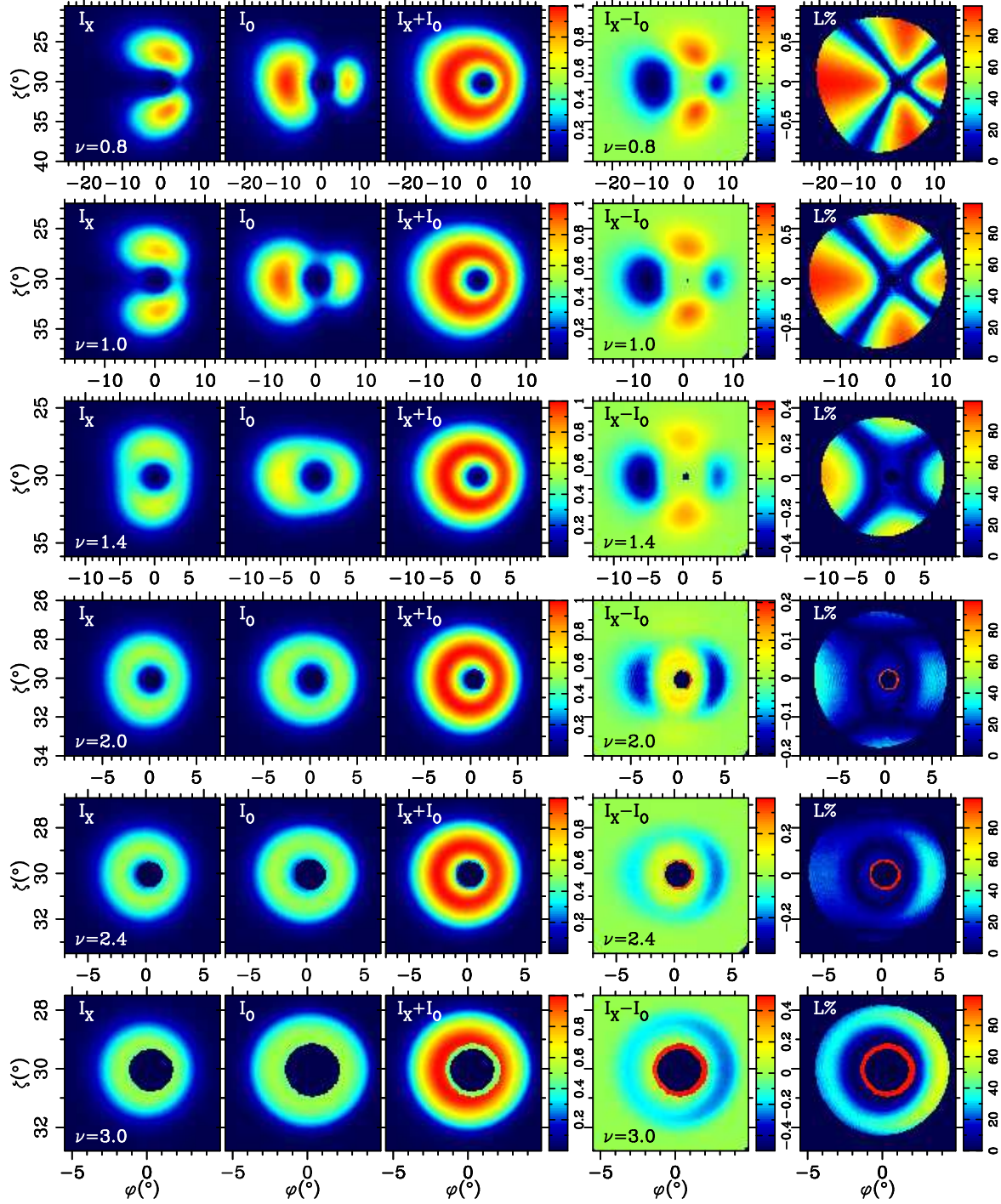


Figure 3. Pulsar polarization emission beams at frequencies of $\nu = 0.8\text{GHz}$, 1.0GHz , 1.4GHz , 2.0GHz , 2.4GHz and 3.0GHz from top to bottom for the X-mode intensities (I_X), the O-mode intensities (I_O), the total intensity ($I_X + I_O$), their difference ($I_X - I_O$, i.e., the net linear polarization) and the fractional linear polarization ($L\% = |(I_X - I_O)/(I_X + I_O)| \times 100\%$). The fractional linear polarization is plotted for the regions where the total intensity exceeds 1% of the peak intensity. The density distribution for relativistic particles is assumed to be located in a cone at $s_p = 0.5$ and with a width of $\sigma_s = 0.12$. The other parameters used for model calculations are $\alpha = 30^\circ$, $\gamma = 500$, $\eta = 100$, $B_\star = 10^{12}\text{Gs}$ and $P = 1\text{s}$.

the X-mode rotate by 90° . Therefore, incoherent superposition of the orthogonal X-mode and O-mode emission causes depolarization for total radiation power. If the corotation of relativistic particles is not considered, significant depolarization occurs. When the corotation is considered, the net

polarization will reserve polarization features of the stronger mode.

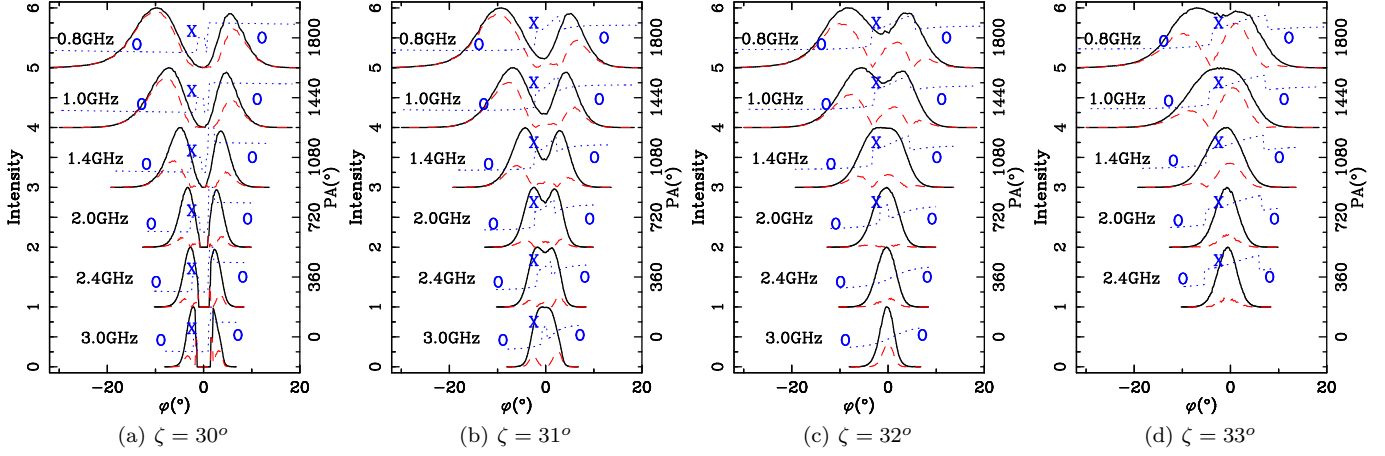


Figure 4. Polarized pulse profiles resulting from cutting of the beams in Fig. 3 by the sight lines at $\zeta = 30^\circ$, 31° , 32° and 33° . The solid lines are for the total intensities, $I_X + I_O$, the dashed lines for the linear polarization intensities, $|I_X - I_O|$, and the dotted lines for position angles of linear polarization. The polarization modes (X or O) are marked near position angle curves.

3 EMISSION AT VARIOUS FREQUENCIES

After knowing emission regions and propagation effects, we can now calculate the polarization states of emission at various frequencies. The wave mode distributions within an entire pulsar beam (the X mode intensity, I_X , the O mode intensity, I_O , total intensity, $I_X + I_O$, and the intensity for the linear polarization, $I_X - I_O$), polarized pulse profiles, and their evolution with frequency can be calculated for the emission generated from different heights for the entire open magnetosphere.

3.1 Emission generated by particles with a single value of the Lorentz factor γ at ν_{CR}

In our calculations, the coherent particle bunch is simply treated as a point-like huge charge. The emission intensity is closely related to local particle densities. Here, the conal-shaped density distribution for particles is adopted as $N(r, \theta, \phi) = N_0 r^{-3} f(\theta) g(\phi)$, with

$$\begin{aligned} f(\theta) &= f_0 \exp\left[-\frac{(s - s_p)^2}{2\sigma_s^2}\right], \\ g(\phi) &= 1. \end{aligned} \quad (3)$$

Here, $s = \theta_c / \theta_{c,max}$, θ_c is the polar angle of a field line footed on the neutron star surface, $\theta_{c,max} = \sin^{-1}(\sqrt{R_*/r_{e,lof}})$ represents the polar angle maximum, i.e., the polar angle for the last open field line footed on the neutron star surface, s_p is the position for density peak¹.

Using such a particle density distribution, we can now get the polarized emission at various frequencies in the model. The steps follow Wang et al. (2012, 2014). First, we find the field lines for emission within the $1/\gamma$ cone pointing towards a given direction. Then, the electric fields of the emission within the cone will be decomposed into the X-mode and O-mode components following the direction of local magnetic field. Evolution of the X-mode and O-mode

components within the $1/\gamma$ cone will be traced until the polarization limiting radii by considering the refraction and the adiabatic walking effects. The integration of emission within each cone will result in the X-mode and O-mode intensities. Finally, emission pointing outwards from the entire open field line region will be mapped. The equations governing the ray trajectory and polarization state evolutions have been given in details in Wang et al. (2014).

In Fig. 3, we show pulsar polarization emission beams for the X-mode, O-mode, total intensity, and the linear polarization at six frequencies of $\nu = 0.8\text{GHz}$, 1.0GHz , 1.4GHz , 2.0GHz , 2.4GHz and 3.0GHz . The beams for low frequency emission are generally larger than those for high frequencies due to a larger opening angle from a higher altitude. Moreover, the X-mode and O-mode dominate different parts of the pulsar beam, i.e., the X-mode dominates at two sides of the beam in ζ direction while the O-mode dominates in ϕ direction, as shown in the panels for I_X and I_O in Fig. 3. Further, emission regions for the X mode and O mode are very distinct for lower frequency emission coming from a higher altitude. With increase of observing frequency, the distribution regions of the two modes gradually overlap, and hence serious depolarization happens, as shown by $I_X - I_O$ and fractional linear polarization of $L\%$ in Fig. 3. The differences are caused mainly by different corotation velocities of relativistic particles. When the corotation of relativistic particles is not considered, the distribution regions for two modes are almost completely overlapped (Wang et al. 2014). The O-mode distribution regions are generally broader than those for the X-mode for the beams at higher frequencies, as shown in Fig. 3, which is caused by the dense plasma in deeper magnetosphere where serious refraction effect results in a prominent outward shift of the O mode beam.

When a given sight line cuts across a pulsar beam, it will find polarized pulse profiles at a series of frequencies, as shown in Fig. 4. For the central cut at $\zeta = 30^\circ$, the observed pulse profiles are predominantly of the O mode except for a small central phase region for the X mode. Emission at a lower frequency, like $\nu = 0.8\text{GHz}$, is highly linearly polarized. With the increase of frequency, the fractional linear polarization, $L\%$, gradually decreases and the profile width,

¹ In this paper the meaning of 's' is the same as ϑ in Wang et al. (2014).

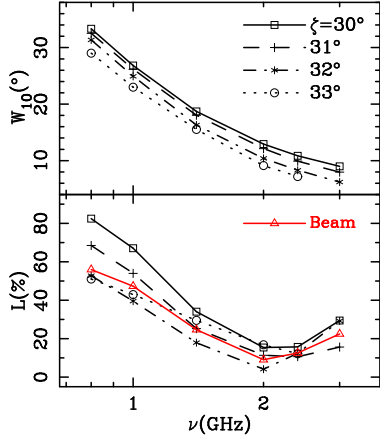


Figure 5. Evolution of fractional linear polarization $L\%$ and profile width W_{10} with frequency. The fractional linear polarizations are calculated for the profiles in Fig. 4 with the sight lines of $\zeta = 30^\circ, 31^\circ, 32^\circ$ and 33° at frequencies $\nu = 0.8, 1.0, 1.4, 2.0, 2.4$ and 3.0 GHz. The red solid line represent the fractional linear polarizations for the entire beams in Fig. 3 with the total intensity above 1% the peak intensity. The model parameters are the same as those in Fig. 3, i.e., $\alpha = 30^\circ, \gamma = 500, \eta = 100, B_* = 10^{12}$ Gs and $P = 1$ s.

W_{10} , narrows down correspondingly, as shown in Fig. 5. As observing frequency further increases to about 3.0 GHz, the pulse profile keeps narrowing down, but the fractional linear polarization increases. This is because the refraction effect becomes stronger as the plasma density increases, which dominates over the influence of rotation in determining pulsar linear polarization. The frequency dependencies of fractional linear polarization and profile width are similar for different sight lines, such as $\zeta = 31^\circ, 32^\circ$ and $\zeta = 33^\circ$. Moreover, the fractional linear polarization of the entire pulse beam exhibits a similar frequency dependence as those for the above discussed pulse profiles, which is outlined by the red solid line in Fig. 5.

The frequency dependencies of fractional linear polarization and profile width are also calculated for plasmas with various Lorentz factors γ and multiplicity parameters η , as shown in Fig. 6. It can be seen from Fig. 6(a) that profile widths decrease with the increase of frequency, but the fractional linear polarization decreases first and then may increase, similar to those in Fig. 5, except that the lower frequency emission is generated by relativistic particles with a smaller Lorentz factor. If particles have larger Lorentz factors, emission of a given frequency will be generated in higher magnetosphere. Because the rotation has already separated the distribution regions for the X and O modes above a certain height, emission above the height will be highly polarized with an almost constant polarization degree, as shown in Fig. 6(b). We can know from Fig. 6(c) and (d) that high frequency emission generated in a dense plasma with a large η in deeper magnetosphere tends to have a larger fraction of linear polarization than those in less dense plasma with a small η . This is caused by mode separation induced by the O-mode refraction, the effect is proportional to η (Barnard & Arons 1986).

In summary, with curvature radiation mechanism, the radiation keeps highly linearly polarized at low frequen-

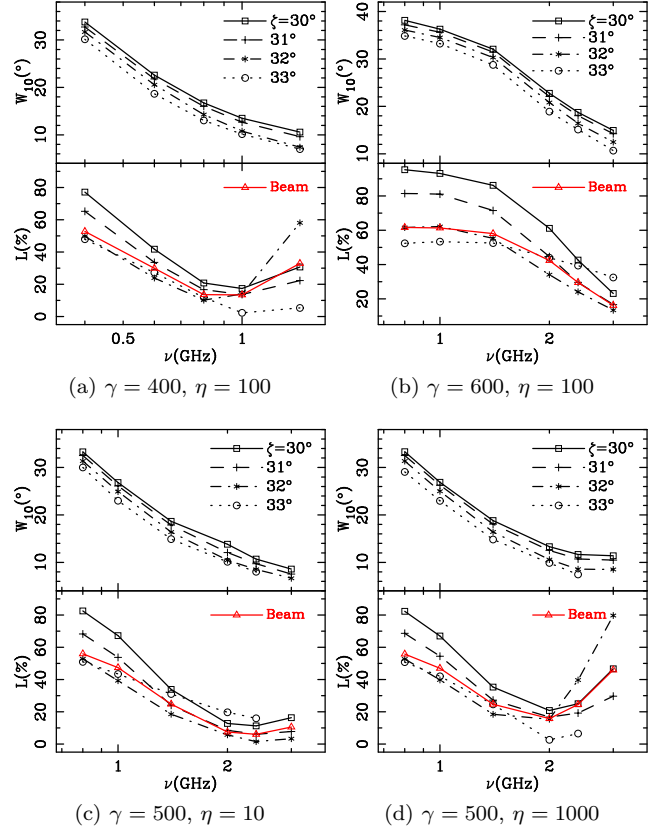


Figure 6. Same as Fig. 5 except for particles with different Lorentz factor γ or density η .

cies. The polarization gradually decreases with observing frequency, but may increase at a very high frequency. The rotation plays an important role in keeping high degree of linear polarization, and can cause the decrease of fractional linear polarization in higher magnetosphere. Serious refraction in a deep magnetosphere, which is significant when the plasma is dense and particles have a small Lorentz factor, will lead a larger fraction of linear polarization for high frequency emission.

3.2 Emission generated from a region of the same height

We have investigated the frequency dependence of pulsar linear polarization emitted at the characteristic frequency ν_{CR} . Curvature radiation from a relativistic particle or a particle bunch has a spectrum which is a power law with an index of $1/3$ at the lowest frequency and decreases exponentially at high frequencies, not just at the frequency of ν_{CR} . Hence, emission of various frequencies may be produced from the region of the same height in a pulsar magnetosphere.

For investigations conducted here, it is assumed that emission of different frequencies is generated from the region of the same height as the emission of $\nu_{CR} = 1.0$ GHz. For a given ν_{CR} , the shape of curvature radiation spectrum can be uniquely determined. Therefore, emission of different frequencies has the same beam pattern. However, due to the influence of frequency dependent propagation effects, the final beam patterns will be modified. As done in the

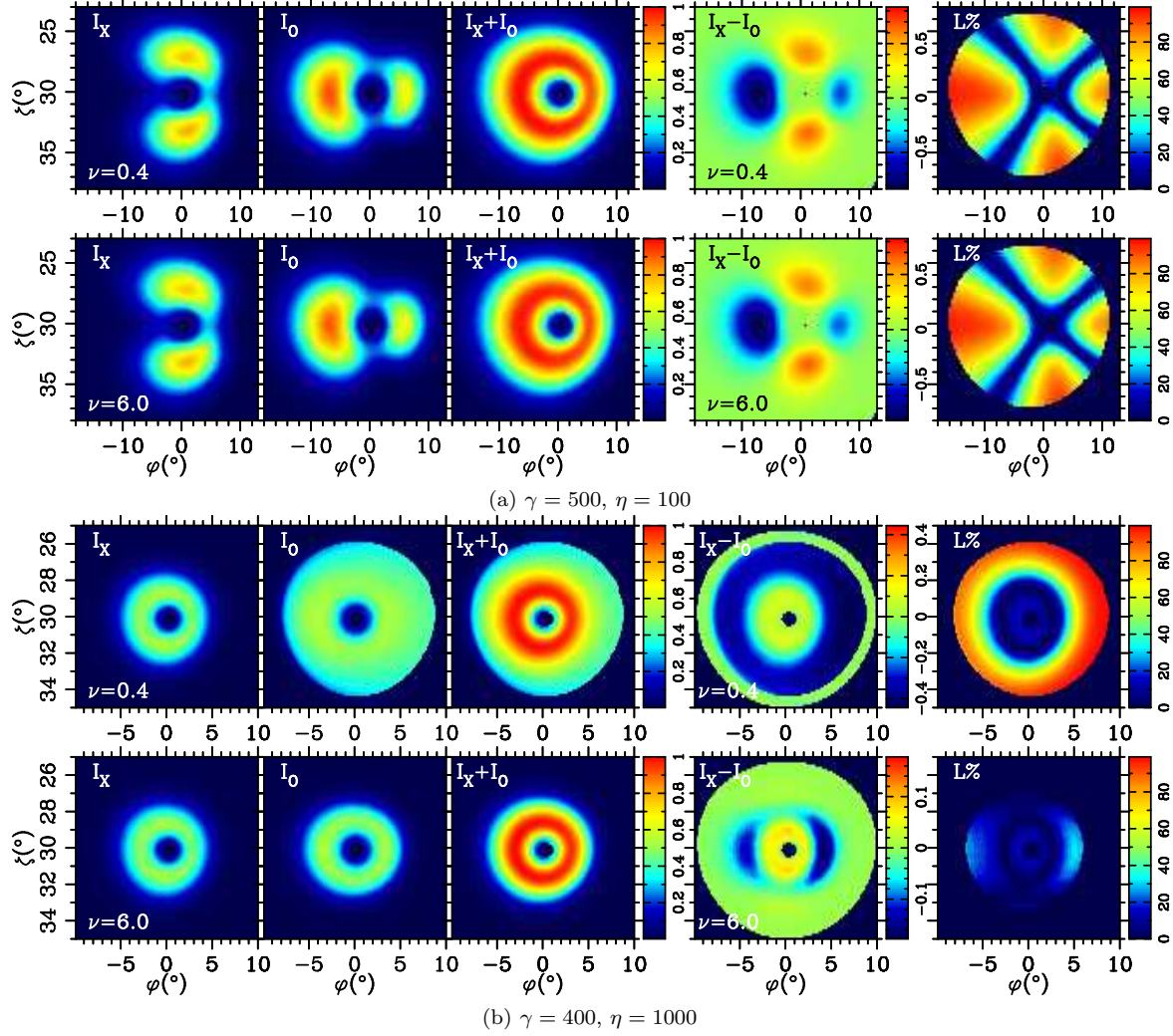


Figure 7. Same as Fig. 3 for polarization beams but with different parameters. Panels (a) are for the plasma with $\gamma = 500$ and $\eta = 100$. Emission at frequencies of 0.4 and 6.0 GHz is generated from the same height region as the emission of $\nu_{\text{CR}} = 1.0$ GHz. Panels (b) are for the plasma with $\gamma = 400$ and $\eta = 1000$. The other parameters used for model calculations are the same as those in Fig. 3, i.e., $\alpha = 30^\circ$, $B_\star = 10^{12}$ Gs and $P = 1$ s.

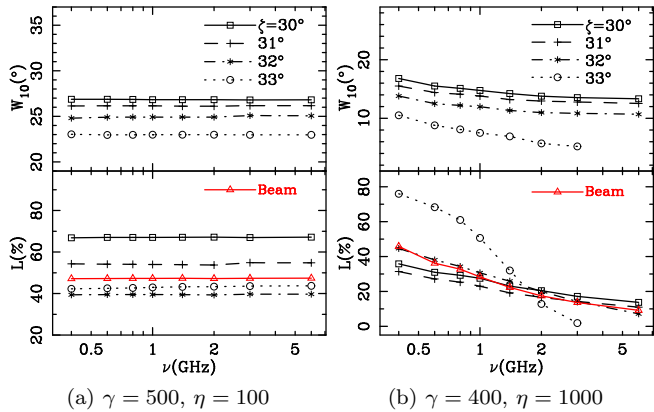


Figure 8. Same as Fig. 5 but for (a) Lorentz factor $\gamma = 500$ and plasma density $\eta = 100$, and (b) Lorentz factor $\gamma = 400$ and plasma density $\eta = 1000$. The fractional linear polarization and profile width are calculated by cutting the beams in Fig. 7.

previous section, we calculate intensity distributions of the two mode within the entire pulsar beam, and then polarized pulse profiles for various frequencies and sight line angles, and finally find the corresponding frequency dependencies of fractional linear polarization and profile width, as shown in Figs. 7 and 8.

For moderate plasma conditions with a Lorentz factor of $\gamma = 500$ and a density of $\eta = 100$, the wave mode distributions within a pulsar beam are similar for various frequencies, as shown in Fig. 7 (a). The profile widths and fractional linear polarizations almost do not change with frequency, as shown in Fig. 8 (a). This kind of frequency dependence is caused by the fact that the effects of rotation are the same for emission of different frequencies, because they are generated from the same height region, and the O mode components are less affected by the refraction effect. If the plasma has a smaller Lorentz factor of $\gamma = 400$ but with a larger density of $\eta = 1000$, the distribution regions for the X and O modes are overlapped, and the refraction effect becomes much more significant, especially for lower frequency

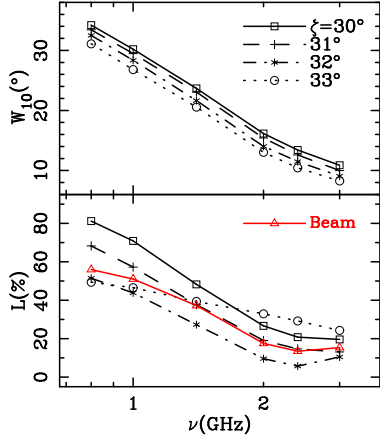


Figure 9. Same as Fig. 3 except for particles with a gaussian distribution of energy, with $\gamma_m = 500$, and $\sigma_\gamma = 50$.

emission (Barnard & Arons 1986; Wang et al. 2014). It results in broader distribution regions for O mode than those for X mode, as shown in Fig. 7 (b). Compared with emission at 6.0GHz, the O mode distribution region for emission at 0.4 GHz is even much broadened. Therefore, both the profile width and fractional linear polarization decrease with frequency. This frequency dependence is due to that polarization features at higher frequencies are generated in deeper magnetosphere within a small altitude range. Our result is contrary to the argument given by McKinnon (1997) that the refraction causes average pulse profiles to depolarize while the profile width remains a constant.

3.3 Emission generated by particles with γ distribution

The frequency dependence of pulsar emission has been considered for curvature radiation of relativistic particles with a single γ in the regions with either a range of heights or the same height. Relativistic particles within a pulsar magnetosphere generated by the sparking process may have an energy distribution (Medin & Lai 2010), which we assume to be $N(\gamma) \sim \exp[-(\gamma - \gamma_m)/2\sigma_\gamma^2]$. Doing the same as previous subsections, we get intensities and polarizations of wave modes within the entire pulsar beam for each discrete Lorentz factor, and then sum them incoherently for total radiation. The polarized pulse profiles and their frequency dependencies are calculated, as shown in Fig. 9, which are similar to those for the relativistic particles with a single γ shown in Fig. 3. The frequency dependence here becomes less steep. Depolarization, which is caused by addition of emission by relativistic particles with different Lorentz factors, leads emission at 3.0GHz to be less polarized compared to emission produced by particles with a single γ .

4 COMPARISON WITH OBSERVATIONS

We have numerically simulated wave mode distribution regions and polarization beams, calculated polarized pulse profiles and their evolution with frequency for the conal-shaped density model with various plasma conditions. We have demonstrated the frequency dependent depolarization

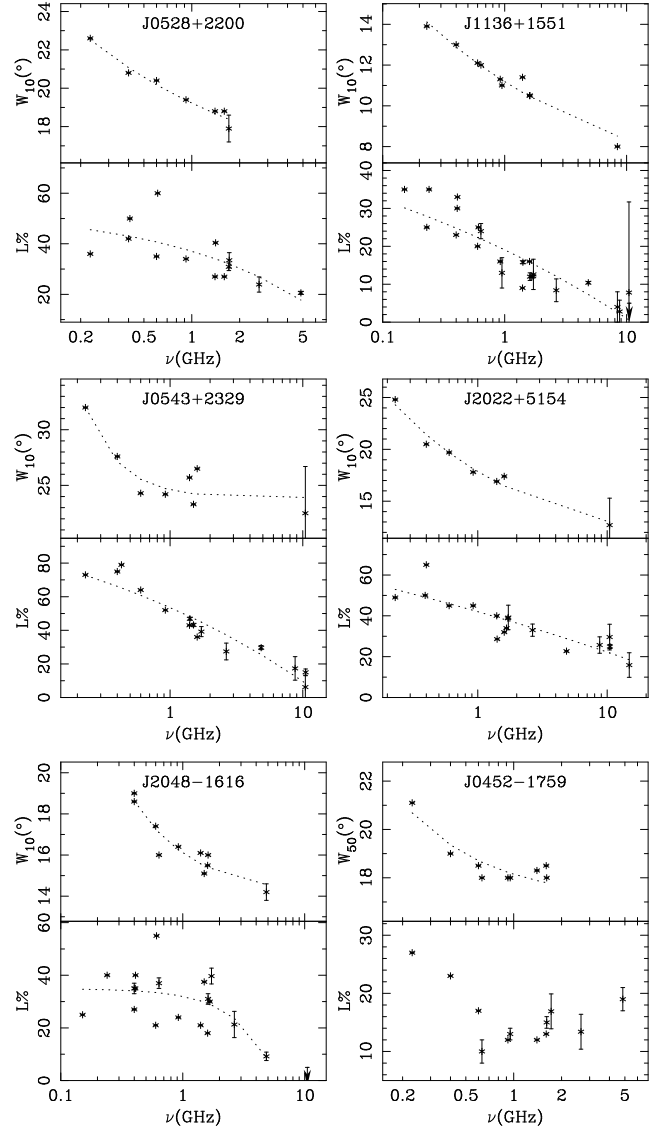


Figure 10. The profile widths, W_{10} , and fractional linear polarizations, $L\%$, at a series of frequencies. The data are collected from literatures as listed in Table 1. The dotted lines represent model fitting.

without loss of generality. In general, the fractional linear polarization together with profile width decrease with frequency. In order to check the validity of our simulations, it is worthwhile to compare our results with pulsar polarization observations.

Fig. 10 shows the changes of observed profile widths and fractional linear polarizations for six pulsars at a series of frequencies, with the data collected in table 1 in appendix from literatures. These pulsars are of different morphological types (Rankin 1983; Lyne & Manchester 1988). **PSR J0528+2200** and **J1136+1551** are conal double pulsars, each of which has two well separated conal components and smoothly varied position angle curves. **PSR J0543+2329** and **J2022+5154** belong to the type of partial cone, which has only one conal component and represents one side of conal emission as indicated by position angle curve. **PSR J2048-1616** is a triple-component pulsar. It has two conal

components at the outer parts of pulse profiles and one core component in middle. With increasing frequency, the central core component gradually disappears as it has a steeper spectrum (Rankin 1983). **PSR J0452-1759** has multiple components.

The evolution of profile width and fractional linear polarization with frequency can be interpreted for these pulsars by combing the curvature radiation processes together with propagation effects within pulsar magnetosphere. The widths of all these pulsars decrease with frequency. A constant plus a power law, $W_{10} = W_c + (\nu/\nu_0)^a$, can account for the frequency dependence, as pointed out by Thorsett (1991). The frequency dependence of pulse width or beam width can be understood in the frame of curvature radiation mechanism by involving the density and energy distributions of relativistic particles within a pulsar magnetosphere (Wang et al. 2013). The fractional linear polarization is found to decrease with frequency as well. A constant minus a power law, $L = L_c - (\nu/\nu_0)^b$, can be used to fit the frequency dependence, as indicated by dotted lines in Fig. 10, which could result from depolarization by addition of the X mode and O mode as discussed in section 3.1 and 3.2. However, the fractional linear polarization of PSR J0452-1759 decreases first and then increases, and the increase of fractional linear polarization may be due to the significant refraction effect, as discussed in section 3.1.

5 DISCUSSIONS AND CONCLUSIONS

In this paper, we have investigated the frequency dependence of pulsar linear polarization by considering the curvature radiation process together with propagation effects. The X and O mode distributions within the entire pulsar beam, polarized pulse profiles and their evolution with frequency are calculated for emission at different frequencies originated from regions of different or the same height in a pulsar magnetosphere. We find the following conclusions:

(i) Rotation can lead to the separation of distribution regions for the X and O mode within a pulsar beam, the effect of which is much more significant for low frequency emission generated at higher magnetosphere.

(ii) The fractional linear polarization tends to approach a constant degree towards low frequency limit, as the distribution regions of the two modes have almost been separated above certain heights.

(iii) The fractional linear polarization generally decreases with frequency. Because the higher frequency emission is generated from a lower altitude, where rotation induced mode separation is not significant.

(iv) The fractional linear polarization could increase at higher frequency due to the significant O mode refraction.

(v) If emission originates from almost the same height region, the O mode refraction will lead to the decrease of profile width and fractional linear polarization with frequency. The refraction influence is much more significant if the plasma has a large density or a small Lorentz factor.

(vi) Depolarization caused by the randomization of polarized emission from different heights of pulsar magnetosphere is obvious for high frequency emission generated from the hot relativistic plasma. However, it does not change the

basic tendency of which the fractional linear polarization decrease with frequency.

The model simulations in this paper may help us to understand some statistical features of pulsar linear polarization. For short period pulsars, relativistic particles within the magnetosphere may suffer much more significant rotation influences. Hence, the X mode and O mode distribution regions tend to be separated and the pulsars may have higher linear polarization. The relativistic particles of high \dot{E} pulsars may be accelerated to a very higher energy (larger γ). Their emission can be generated from a much higher magnetosphere, where the significant rotation will also lead to a large fraction of linear polarization.

In our calculations, the frequency dependence of emission region is determined by referring to the characteristic frequency of curvature radiation, and emission intensities are closely related to local plasma density. However, emission intensities depend on the detailed coherent process within pulsar magnetosphere, which is not yet resolved now. Moreover, our calculations simply assume that streams of relativistic plasmas are cold and distributed in a conal shaped region, which travel along the curved dipole magnetic field lines and corotate with a pulsar magnetosphere. However, the actual energy and density distributions of particles are unknown, which can be hot and with irregular density shapes (Medin & Lai 2010). Furthermore, due to the influences of rotation and polar cap current, pulsar magnetosphere may be of distorted dipole form (Kumar & Gangadhara 2013), which may affect pulsar polarization states and is not yet considered in this paper.

Pulsars exhibit rich diversities of polarization profiles, some of which are not consistent with our model predictions. For example, the profile width of PSR J1239+2453 decreases with observing frequency, but its fractional linear polarization increase first and then decrease; the profile widths of PSR J0601-0527 decrease but their fractional linear polarizations increase; the profile width and fractional linear polarization for PSR J2113+4644 increase. Moreover, individual profile components of a given pulsar can behave differently with frequency (Johnston et al. 2008). For example, the highly polarized profile component of PSR J0922+0638 remain highly polarized at high frequencies. These diverse polarization features need further investigations.

ACKNOWLEDGEMENTS

This work has been supported by the National Natural Science Foundation of China (11403043, 11473034 and 11273029), and the Strategic Priority Research Program ‘The Emergence of Cosmological Structures’ of the Chinese Academy of Sciences (Grant No. XDB09010200).

REFERENCES

- Barnard J. J., Arons J., 1986, *ApJ*, 302, 138
- Biggs J. D., 1990, *MNRAS*, 245, 514
- Beskin V. S., Philippov A. A., 2012, *MNRAS*, 425, 814
- Cheng A. F., Ruderman M. A., 1979, *ApJ*, 229, 348
- Crawford F., Manchester R. N., Kaspi V. M., 2001, *AJ*, 122, 2001

Dyks J., Rudak B., Demorest P., 2010, MNRAS, 401, 1781
 Gangadhara R. T., 2004, ApJ, 609, 335
 Goldreich P., Julian W. H., 1969, ApJ, 157, 869
 Gould D. M., Lyne A. G., 1998, MNRAS, 301, 235
 Hamilton P. A., McCulloch P. M., Ables J. G., Komesaroff M. M., 1977, MNRAS, 180, 1
 Han J. L., Demorest P. B., van Straten W., Lyne A. G., 2009, ApJS, 181, 557
 Huguenin G. R., Manchester R. N., Taylor J. H., 1971, ApJ, 169, 97
 Johnston S., Karastergiou A., Mitra D., Gupta Y., 2008, MNRAS, 388, 261
 Johnston S., Karastergiou A., Willett K., 2006, MNRAS, 369, 1916
 Karastergiou A., Johnston S., Manchester R. N., 2005, MNRAS, 359, 481
 Kumar D., Gangadhara R. T., 2012, ApJ, 746, 157
 Kumar D., Gangadhara R. T., 2013, ApJ, 769, 104
 Lyne A. G., Manchester R. N., 1988, MNRAS, 234, 477
 Lyne A. G., Smith F. G., Graham D. A., 1971, MNRAS, 153, 337
 Manchester R. N., 1971, ApJS, 23, 283
 Manchester R. N., Hamilton P. A., McCulloch P. M., 1980, MNRAS, 192, 153
 Manchester R. N., Taylor J. H., Huguenin G. R., 1973, ApJL, 179, L7
 Manchester R. N., Taylor J. H., Huguenin G. R., 1975, ApJ, 196, 83
 McCulloch P. M., Hamilton P. A., Manchester R. N., Ables J. G., 1978, MNRAS, 183, 645
 McKinnon M. M., 1997, ApJ, 475, 763
 McKinnon M. M., Stinebring D. R., 1998, ApJ, 502, 883
 Medin Z., Lai D., 2010, MNRAS, 406, 1379
 Morris D., Graham D. A., Sieber W., 1981, A&A, 100, 107
 Morris D., Graham D. A., Sieber W., Bartel N., Thomasson P., 1981, A&AS, 46, 421
 Morris D., Schwarz U. J., Cooke D. J., 1970, ApL, 5, 181
 Qiao G. J., Manchester R. N., Lyne A. G., Gould D. M., 1995, MNRAS, 274, 572
 Rankin J. M., 1983, ApJ, 274, 333
 Rankin J. M., Benson J. M., 1981, AJ, 86, 418
 Thorsett S. E., 1991, ApJ, 377, 263
 Tiburzi C., Johnston S., Bailes M., et al. 2013, MNRAS, 436, 3557
 van Ommen T. D., D'Alessandro F., Hamilton P. A., McCulloch P. M., 1997, MNRAS, 287, 307
 von Hoensbroech A., Kijak J., Krawczyk A., 1998, A&A, 334, 571
 von Hoensbroech A., Lesch H., Kunzl T., 1998, A&A, 336, 209
 von Hoensbroech A., Xilouris K. M., 1997, A&AS, 126, 121
 Wang C., Lai D., Han J. L., 2010, MNRAS, 403, 569
 Wang P. F., Han J. L., Wang C., 2013, ApJ, 768, 114
 Wang P. F., Wang C., Han J. L., 2012, MNRAS, 423, 2464
 Wang P. F., Wang C., Han J. L., 2014, MNRAS, 441, 1943
 Weltevrede P., Johnston S., 2008, MNRAS, 391, 1210
 Wu X. J., Manchester R. N., Lyne A. G., Qiao G., 1993, MNRAS, 261, 630
 Xilouris K. M., Kramer M., Jessner A., Wielebinski R., Timofeev M., 1996, A&A, 309, 481
 Xilouris K. M., Seiradakis J. H., Gil J., Sieber W., Wielebinski R., 1995, A&A, 293, 153

Xu R. X., Liu J. F., Han J. L., Qiao G. J., 2000, ApJ, 535, 354

APPENDIX

Table 1. The profile width, W_{10} , and the fractional linear polarization, $L\%$, at various frequencies for six pulsars.

PSR Jname	Freq.(GHz)	$W_{10}(^{\circ})$	$L\%$	Ref
J0452-1759 [†]	0.23	21.1	27	1
	0.4	19	23	1
	0.6	18.5	17	1
	0.631	18	10 ± 2	6
	0.92	18	12	1
	0.95	18	13 ± 1	10
	1.4	18.3	12	1
	1.6	18.5	13	1
	1.612	18	15 ± 1	7
	1.72	-	16.9 ± 3	8
	2.65	-	13.4 ± 3	8
	4.85	-	19 ± 2	11
J0528+2200	0.23	22.6	36	1
	0.4	20.8	42	1
	0.408	-	50	4
	0.6	20.4	35	1
	0.61	-	60	4
	0.92	19.4	34	1
	1.4	18.8	27	1
	1.41	-	40.4 ± 0.2	12
	1.6	18.8	27	1
	1.71	17.9 ± 0.7	30.9 ± 1.5	12
	1.72	-	33.5 ± 3	8
	2.65	-	23.9 ± 3	8
	4.85	-	20.6 ± 0.6	12
J0543+2329	0.23	32.0	73	1
	0.4	27.6	75	1
	0.43	-	79	9
	0.6	24.3	64	1
	0.92	24.2	52	1
	1.4	25.7	43	1
	1.41	-	46.9 ± 0.9	12
	1.5	23.3	43.2 ± 1.0	13
	1.6	26.5	36	1
	1.72	-	39.2 ± 3	8
	2.65	-	27.4 ± 5	8
	4.85	-	29.7 ± 1.2	12
	8.75	-	17.3 ± 7	8
	10.45	22.5 ± 4.2	6.2 ± 7.1	12
	10.55	-	15 ± 2	14
J1136+1551	0.151	-	35	4
	0.23	13.9	25	1
	0.24	-	35	4
	0.4	13.0	23	1
	0.408	-	30	4
	0.41	-	33	5
	0.6	12.1	20	1
	0.61	-	25	4
	0.638	12	24 ± 2	6
	0.92	11.3	16	1
	0.95	11	13 ± 4	10
	1.4	11.4	9	1
	1.41	-	15.8 ± 0.4	12
	1.6	10.5	16	1
	1.612	10.5	12 ± 1	7
	1.665	-	12	5
	1.71	-	12.1 ± 0.2	12
	1.72	-	12.6 ± 4	8
	2.65	-	8.4 ± 3	8
	4.85	-	10.4 ± 0.3	12
	8.4	8	4 ± 4	3
	8.75	-	2.8 ± 3	8
	10.45	-	7.8 ± 23.9	12
	10.55	-	≤ 5	14
J2048-1616	0.151	-	25	4
	0.24	-	40	4
	0.4	18.6	27	1
	0.4	19	35 ± 2	2
	0.408	-	35	4
	0.41	-	40	5
	0.6	17.4	21	1
	0.61	-	55	4
	0.638	16	37 ± 2	6
	0.92	16.4	24	1
	1.4	16.1	21	1
	1.5	15.1	37.5 ± 0.1	13
	1.6	15.5	18	1

	1.612	16	31 ± 2	7
	1.665	-	30	5
	1.72	-	39.7 ± 3	8
	2.65	-	21.3 ± 5	8
	4.85	14.2 ± 0.4	9.2 ± 1.6	12
	10.55	-	≤ 5	14
J2022+5154	0.23	24.8	49	1
	0.392	-	50	5
	0.4	20.5	65	1
	0.6	19.7	45	1
	0.92	17.8	45	1
	1.4	16.9	40	1
	1.41	-	28.6 ± 0.1	12
	1.6	17.4	32	1
	1.665	-	34	5
	1.71	-	38.8 ± 0.3	12
	1.72	-	39.2 ± 6	8
	2.65	-	33 ± 3	8
	4.85	-	22.7 ± 0.3	12
	8.75	-	25.7 ± 4	8
	10.45	12.7 ± 2.6	29.6 ± 6.3	12
	10.5	-	25 ± 1	14
	14.8	-	15.9 ± 6	8

Notes. [†] The widths of PSR J0452-1759 are exceptionally measured at 50% of the peak intensities. References for previous polarization observations: ¹Gould & Lyne (1998), ²Hamilton et al. (1977), ³Johnston et al. (2006), ⁴Lyne et al. (1971), ⁵Manchester (1971), ⁶McCulloch et al. (1978), ⁷Manchester et al. (1980), ⁸Morris et al. (1981), ⁹Rankin & Benson (1981), ¹⁰van Ommen et al. (1997), ¹¹von Hoensbroech et al. (1998), ¹²von Hoensbroech & Xilouris (1997), ¹³Weltevrede & Johnston (2008), ¹⁴Xilouris et al. (1995).